Biosensors and Bioelectronics 311 (2026) 118952

Contents lists available at ScienceDirect

Biosensors and Bioelectronics

journal homepage: www.elsevier.com/locate/bios

Binary spatial-spectral encoding and decoding for ultra-multiplexed digital PCR: Breaking the fluorescence channel limit

Jinrong Shen [a,1], Jingxing Fan [a,1], Gangwei Xu [b], Zhehao Zhao [b], Haofeng Li [a], Dongping Wu [a,*]

[a] State Key Laboratory of Integrated Chips and Systems, College of Integrated Circuits and Micro-Nano Electronics, Fudan University, Shanghai, 200433, China
[b] Shanghai Turtle Technology Limited, Shanghai, 200444, China

ARTICLE INFO

Keywords:
Ultra-multiplexed digital PCR
Binary spatial-spectral encoding
Partition-resolved decoding
Partition identity preservation
Decoding robustness

ABSTRACT

Digital PCR (dPCR) is widely used for absolute nucleic acid quantification because of its high sensitivity and precision. Its major implementations include droplet-based digital PCR (ddPCR), which generates stochastic droplet partitions, and chip-based digital PCR (cdPCR), which uses fixed-position microchamber arrays. Despite their different partition architectures, both formats remain fundamentally limited in multiplexing capacity by the number of available fluorescence channels (N). Existing strategies, such as amplitude modulation and probe-ratio encoding, partially increase capacity, but their reliance on analog fluorescence stratification makes them increasingly vulnerable to signal variation, spectral crosstalk, and cluster overlap as the target number increases.

Here, we propose a binary spatial-spectral encoding and decoding framework for ultra-multiplexed dPCR. The strategy constructs target identities from the binary ON/OFF fluorescence states of the same spatially indexed partition across channels, expanding the theoretical detection capacity from N to 2^N-1. The key requirement is reliable preservation of partition identity across multi-channel readout. In this study, cdPCR was used as the first implementation platform because its fixed-position architecture naturally supports chamber-resolved cross-channel correspondence.

Using this framework, we achieved simultaneous detection of nine respiratory pathogens with four fluorescence channels while maintaining accurate quantification across four orders of magnitude ($R^2 = 0.9998$). These results establish binary spatial-spectral decoding as a scalable strategy for multiplex dPCR, with potential extension to ddPCR through reliable cross-channel droplet tracking or re-identification.

1. Introduction

Digital PCR (dPCR) has become an important platform for absolute nucleic acid quantification because of its high sensitivity, precision, and robustness against amplification-efficiency variation(Sanders et al., 2011; Vogelstein and Kinzler, 1999; Whale et al., 2012; Xu et al., 2023). By partitioning a sample into thousands of independent micro-reactions and applying Poisson statistics to endpoint readout, dPCR enables highly sensitive molecular detection and quantification(Heyries et al., 2011; Zhou et al., 2020; Zhu et al., 2017). Owing to these advantages, dPCR has been widely applied in pathogen detection, rare mutation analysis, and molecular diagnostics(Huggett et al., 2015; Mirabile et al., 2024; Zonta et al., 2016).

At present, dPCR is mainly implemented through two major technological routes: droplet-based digital PCR (ddPCR) and chip-based digital PCR (cdPCR)(Olmedillas-López et al., 2022). In ddPCR, samples are partitioned into large numbers of droplets generated by microfluidic emulsification or related approaches, and the resulting partitions may be interrogated by flow-based, scan-based, or imaging-based readout depending on the platform. This format offers high partition throughput, mature commercial instrumentation, and broad adoption in research and diagnostic settings(Li et al., 2018; Suo et al., 2020). In cdPCR, by contrast, reaction mixtures are compartmentalized into predefined microchambers or microwells arranged at fixed spatial positions on a chip(Huang et al., 2023; Morcia et al., 2024). This architecture is highly compatible with imaging-based readout and enables direct association between fluorescence signals and physical partition locations. Thus, although ddPCR and cdPCR share the same digital quantification principle, they differ substantially in partition organization, readout mode, and the manner in which partition identity

* Corresponding author. State Key Laboratory of Integrated Chips and Systems, Fudan University, Shanghai, 200433, China.
E-mail address: dongpingwu@fudan.edu.cn (D. Wu).
[1] These authors contributed equally: Jinrong Shen, Jingxing Fan.

https://doi.org/10.1016/j.bios.2026.118952
Received 30 April 2026; Received in revised form 14 June 2026; Accepted 22 June 2026
Available online 22 June 2026

can be preserved or revisited during analysis.

Despite the broad utility of dPCR, its multiplexing capacity remains fundamentally constrained by the number of available fluorescence channels (N). In conventional one-target-per-channel designs, the number of detectable targets is approximately limited to N(Baker, 2012; Basu, 2017; Li et al., 2024; Schlenker et al., 2021). To overcome this bottleneck, several intensity-based multiplexing strategies have been developed, including amplitude modulation, probe-ratio encoding, and related multi-level fluorescence schemes(Busato et al., 2025; Cao et al., 2025; Gaňová et al., 2021; Trypsteen et al., 2015). These approaches increase detection capacity by introducing multiple fluorescence levels within individual channels, and in some cases can extend multiplexing to approximately 2N(McDermott et al., 2013; Miotke et al., 2014; Tan et al., 2023; Zhong et al., 2011). However, their performance depends on stable separation of analog fluorescence clusters. As the number of targets increases, fluorescence populations become more crowded and more difficult to resolve, while spectral crosstalk, optical nonuniformity, reaction variability, and the "rain" phenomenon further increase decoding uncertainty(Kokkoris et al., 2021; Trypsteen et al., 2015). Consequently, increasing the number of analog intensity levels does not provide a sufficiently robust route toward ultra-multiplexed dPCR(de Korne-Elenbaas et al., 2025; Denis et al., 2016; Wu et al., 2022).

A more general route to expanding multiplexing capacity is to combine spectral information with partition identity(Basu, 2017; Velez et al., 2017; Vynck et al., 2023; Yin et al., 2022). If the same physical partition can be reliably recognized across different fluorescence channels, then channel-wise fluorescence states can be integrated at the partition level and converted into a combinatorial codeword. Under such a framework, multiplexing no longer depends on resolving multiple analog intensity strata within each channel, but instead relies on discrete ON/OFF assignments across channels. Because each channel is classified into a binary state, the decoding process depends primarily on binary separability rather than on precise multi-level fluorescence quantification within a single channel. This transforms target identification into a partition-resolved binary pattern recognition problem and, in principle, expands the theoretical number of assignable non-zero target codewords from N to $2^N - 1$. Conceptually, multiplex expansion may be achieved by integrating spectral states with partition-level identity rather than by further increasing analog fluorescence complexity alone.

In parallel, color-combination dPCR assigns targets predefined fluorophore combinations and identifies them from multichannel fluorescence populations(Santos-Barriopedro et al., 2023). The present framework extends this concept by treating each fixed microchamber as a persistent spatially indexed unit across sequential fluorescence acquisitions. Cross-channel spatial registration enables the complete binary codeword of each chamber to be reconstructed and decoded independently. Thus, the methodological distinction lies in deterministic partition indexing and chamber-resolved spatial-spectral decoding, providing a generalizable architecture that is not restricted to pairwise color combinations.

From this perspective, cdPCR provides a particularly favorable first implementation platform. Because each partition is physically confined to a fixed-position microchamber, the fluorescence signal from the same chamber can be repeatedly acquired and cross-referenced across different spectral windows. This deterministic chamber identity offers a direct physical basis for chamber-resolved signal association and combinatorial encoding. In contrast, ddPCR typically relies on stochastically generated droplets, whose identities are not inherently preserved across repeated readout or multi-step interrogation. Therefore, applying the same framework in ddPCR would require additional strategies, such as droplet immobilization, array-based droplet presentation, image-registration-assisted droplet tracking, or other approaches that enable reliable re-identification of individual droplets across channels or acquisition cycles. These considerations suggest that the proposed method is better viewed as a platform-extensible dPCR framework with different implementation requirements in different partition formats, rather than as a concept intrinsically restricted to cdPCR.

In our previous work, we established a large-field multi-channel fluorescence imaging system for cdPCR with stable full-chip acquisition and high illumination uniformity(Shen et al. 2021, 2025). That platform provided the practical basis for preserving chamber identity across channels and for performing partition-level fluorescence comparison over the full field of view. However, whether such a fixed-position dPCR system could support binary spatial-spectral encoding and decoding beyond the conventional one-target-per-channel readout limit had not yet been investigated.

Here, we propose a binary spatial-spectral encoding and decoding strategy for multiplex digital PCR and demonstrate it on a fixed-position cdPCR platform as a first implementation of partition-resolved identity-preserving decoding. Building on combinatorial fluorescence encoding, the proposed strategy determines target identity by reconstructing the binary ON/OFF codeword of each spatially indexed partition across multiple channels. A large-field multi-channel imaging workflow was used to establish cross-channel chamber correspondence, after which chamber-level fluorescence signals were converted into binary ON/OFF states and assigned predefined combinatorial codewords. In this way, target identity was determined through partition-resolved binary decoding rather than analog intensity stratification. Using this framework, we achieved simultaneous detection of nine respiratory pathogens using only four fluorescence channels while maintaining accurate quantification across four orders of magnitude. Together, these results support a practical route toward identity-preserving multiplex digital PCR beyond conventional one-target-per-channel readout and provide a foundation for extending this strategy to other dPCR formats in the future.

2. Materials and methods

2.1. Simulated clinical sample preparation and cdPCR workflow

For matrix-associated testing, the defined respiratory pathogen target materials were prepared in throat-swab preservation medium, which was used as a simulated clinical matrix. The matrix-containing samples underwent nucleic acid extraction, purification, and concentration before cdPCR analysis. No exogenous inhibitors or off-target nucleic acids were deliberately added, and potential matrix-associated inhibitors were reduced during extraction and purification.

The pathogen abbreviations used throughout the study are as follows: CP, Chlamydia pneumoniae; SP, *Streptococcus pneumoniae*; LP, *Legionella pneumophila*; KP, *Klebsiella pneumoniae*; GAS, group A Streptococcus; MP, *Mycoplasma pneumoniae*; BP, *Bordetella pertussis*; HI, *Haemophilus influenzae*; and Cpsi, Chlamydia psittaci.

The extracted nucleic acids were mixed with the PCR reaction components, including the target-specific primer/probe sets, and then loaded into the cdPCR chip. After partitioning and chip sealing, thermal amplification was performed under the optimized cycling conditions. The amplified chip was subsequently subjected to multi-channel fluorescence imaging, chamber-level binary ON/OFF classification, and spatial-spectral codeword decoding. These samples were used to evaluate the assay following a clinically relevant matrix-processing workflow and were not patient-derived clinical specimens.

2.2. Framework of partition-resolved binary spatial-spectral encoding and its implementation in cdPCR

The proposed framework achieves ultra-multiplexed digital PCR by integrating spectral readout with partition identity. Its central requirement is that the same physical partition can be reliably recognized across different fluorescence channels, so that channel-wise fluorescence states can be combined into a partition-resolved binary codeword. In this way, target identification is no longer based solely on single-channel labeling or analog fluorescence stratification, but on

combinatorial binary signal assignment across multiple spectral windows.

In the present study, this framework was implemented using a chip-based digital PCR (cdPCR) platform because its fixed-position architecture naturally supports deterministic partition indexing (Fig. 1A and B)(Si et al., 2020; Xu et al., 2020). Unlike droplet-based digital PCR (ddPCR), in which partitions are generated stochastically and do not inherently retain spatially addressable identities, the cdPCR chip physically confines reactions within a predefined array of microchambers. The chip adopts a sandwich structure consisting of a top glass layer, a PDMS microchamber layer, and a bottom glass layer, thereby ensuring that each partition occupies a constant physical coordinate throughout the assay. This configuration prevents partition displacement during amplification and imaging, allowing each microchamber to serve as a reusable spatial index across fluorescence channels.

For implementation, the fixed-position cdPCR chip is coupled to a thermal-cycling system, a multichannel excitation module equipped with channel-specific filter sets, and a large-field fluorescence imaging system. Together, these components enable repeated image acquisition and direct cross-channel comparison of the same partitions. As shown in Fig. 1B, fluorescence images are sequentially acquired across multiple channels from the same microchamber array. The resulting fluorescence information can therefore be mapped directly to a defined spatial index rather than inferred from independently generated partitions. By combining deterministic partition positioning with sequential multi-spectral acquisition, the system enables reliable partition-resolved correlation of fluorescence signals across channels, thereby providing the physical basis for binary codeword generation and target decoding. The imaging architecture and platform stability have been described in detail in our previous work.

Although the present study was implemented in a fixed-position cdPCR format, the underlying conceptual framework is not

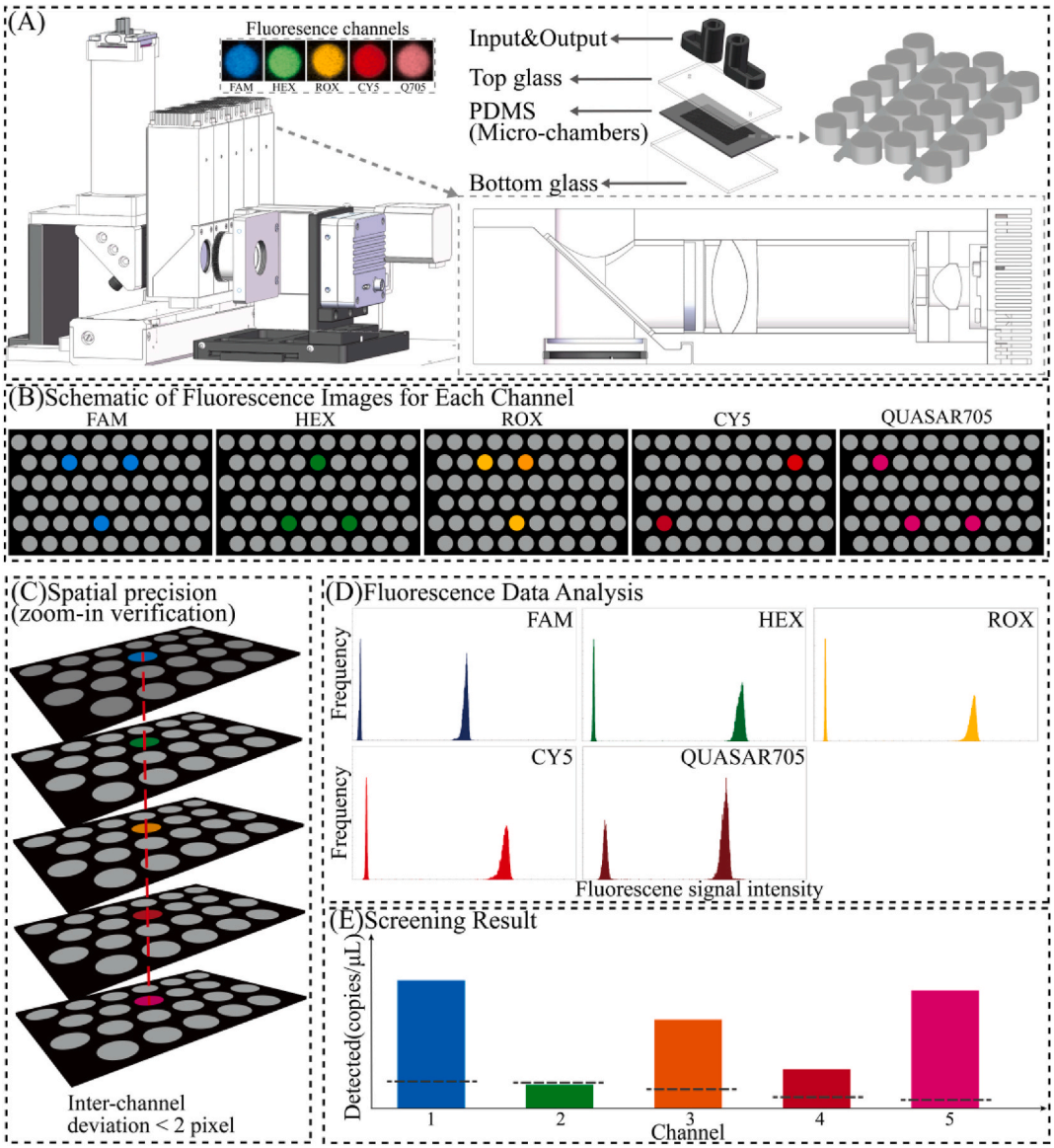

Fig. 1. Framework and implementation workflow of partition-resolved binary spatial-spectral decoding in the cdPCR platform. (A) Schematic of the integrated optical imaging module, cdPCR chip architecture, and illumination configuration used for multi-channel fluorescence acquisition. (B) Sequential acquisition of fluorescence images from the same fixed microchamber array across multiple spectral channels, enabling direct preservation of partition identity during readout. (C) Evaluation of cross-channel spatial consistency based on chamber centroid extraction and spatial indexing. (D) Representative fluorescence intensity distributions of individual channels from calibration measurements, showing the basis for binary threshold assignment. (E) Threshold-based binary decoding workflow for partition-resolved target identification through multi-channel codeword generation and matching.

intrinsically restricted to chip-based systems. In principle, it may also be extended to other dPCR formats if partition identity can be preserved, recovered, or tracked during multi-channel readout.

2.3. Centroid-based spatial indexing and cross-channel consistency evaluation

Because binary target codewords are assigned at the partition level, preservation of partition identity across different fluorescence channels is a fundamental prerequisite for reliable decoding. In this study, we employed a centroid-based localization strategy to quantitatively evaluate spatial consistency across the spectral windows of the cdPCR platform (Fig. 1C).

Individual microchambers were first localized to determine their precise locations within each fluorescence image. The geometric centroid was calculated and defined as the unique spatial index for each chamber. To quantify the spatial correspondence across the full field of view, all centroid coordinates were expressed within a unified global coordinate system. Specifically, for the i-th chamber detected in channels m and n, the centroid deviation $d_i^{(m,n)}$ is defined as:

$$d_i^{(m,n)} = \sqrt{\left(x_i^{(m)} - x_i^{(n)}\right)^2 + \left(y_i^{(m)} - y_i^{(n)}\right)^2} \tag{1}$$

where $\left(x_i^{(m)}, y_i^{(m)}\right)$ and $\left(x_i^{(n)}, y_i^{(n)}\right)$ represent the centroid coordinates of the same physical chamber in channels *m* and *n*, respectively. The distribution of these Euclidean distances across the entire microchamber array was used to determine whether the geometric rigor required for chamber-level spatial-spectral decoding was satisfied(Lau et al., 2017). Unless otherwise specified, centroid deviations reported in the Results refer to the aligned coordinate system used for downstream chamber-level decoding.

For the extended registration analysis, centroid deviations were calculated for all ten channel pairs across 21,384 matched chambers. The edge field was defined as the outer 10% of the coordinate span in either image dimension. The 2-pixel level was used as a reference for registration precision, rather than a failure threshold. Based on the minimum nearest-neighbor chamber spacing of 32 pixels, half of this distance (16 pixels) was used as the geometric potential-misassignment boundary, and deviations reaching this boundary were classified as registration failures.

This analysis establishes the spatial registration basis for subsequent multi-channel binary decoding. More importantly, it defines spatial consistency not merely as an imaging-quality descriptor, but as a core implementation condition for partition-resolved encoding in fixed-position dPCR systems.

2.4. Binary spatial-spectral encoding and partition-resolved decoding

For each fluorescence channel, chamber-level intensities exhibited bimodal distributions corresponding to negative and positive clusters (Fig. 1D). Channel-specific thresholds were determined from the separation between negative and positive intensity populations in calibration measurements to ensure robust classification while minimizing misassignment due to intensity overlap. For the *i*-th chamber in the *m*-th fluorescence channel, the binary fluorescence state $b_i^{(m)}$ was defined as:

$$b_i^{(m)} = \begin{cases} 1, I_i^{(m)} \geq T^{(m)} \\ 0, I_i^{(m)} < T^{(m)} \end{cases} \tag{2}$$

where $I_i^{(m)}$ represents the measured fluorescence intensity and $T^{(m)}$ denotes the threshold for channel *m*.

For a partition-resolved decoding system with N fluorescence channels, each partition can be represented by an N-bit binary fluorescence vector,

$$b_i = \left(b_i^{(1)}, b_i^{(2)}, \ldots, b_i^{(N)}\right), b_i^{(m)} \in \{0, 1\} \tag{3}$$

where $b_i^{(m)}$ denotes the binary ON/OFF state of partition i in channel m. Since each channel has two possible states, the total number of possible binary channel-state combinations is:

$$M_{total} = 2^N \tag{4}$$

Among these combinations, the all-zero vector (0, 0, …, 0) corresponds to a partition that is negative in all channels and therefore does not encode any target. Excluding this null state, the theoretical maximum number of non-zero codewords available for target assignment is:

$$M_{\max} = 2^N - 1 \tag{5}$$

Accordingly, the theoretical multiplexing capacity of the proposed binary spatial-spectral decoding framework scales exponentially with the number of fluorescence channels at the decoding level. In practice, however, the achievable multiplexing level may be lower than $M_{\max}$, because only a subset of codewords may be selected to ensure sufficient decoding robustness, inter-codeword separability, and assay compatibility.

To identify the specific target pathogen within each chamber, the binary states across N fluorescence channels were concatenated to generate a chamber-specific codeword (Fig. 1E). Target identities were predefined using an encoding matrix that assigned unique, non-overlapping binary codewords to individual targets (Fig. 4B). Observed chamber codewords were then compared with the predefined encoding matrix to determine the identity of each chamber. The number of positive chambers corresponding to target k was obtained by counting chambers whose codewords matched the predefined target codeword c_k:

$$d_k = \sum_{i=1}^{n} 1(b_i = c_k) \tag{6}$$

where *n* represents the total number of microchambers and 1(·) denotes the indicator function that equals 1when the condition is satisfied and 0 otherwise.

This binary mapping transforms the multiplex detection problem from multi-level analog intensity discrimination into discrete pattern matching at the partition level. In the present cdPCR implementation, decoding was performed at the chamber level; more generally, however, the same principle applies to any dPCR system in which partition identity can be reliably maintained across channels. For broader implementation across assays and platforms, further standardization of threshold calibration and assignment criteria will be important for ensuring decoding consistency under varying experimental conditions.

2.5. Decoding confidence analysis and Poisson-based quantification

To evaluate the reliability of the ultra-multiplexed detection, a decoding confidence metric CI was introduced. Unlike concentration-estimation confidence intervals used in previous color-combination dPCR studies, the present metric is intended to evaluate decoding consistency at the multiplex-pattern level, namely the agreement between observed combinatorial events and their theoretical expectations (Santos-Barriopedro et al., 2023). This metric assesses the consistency between the observed multiplexed positive rates and the theoretical expectations derived from lower-order channel combinations. For a four-channel implementation (N = 4), the theoretical positive rate P_{th} for a specific combinatorial pattern is calculated as:

$$p_{th} = -1 + \sum_{i-1}^{4} r_i - \sum_{1 \leq i \leq j \leq 4} r_{ij} + \sum_{1 \leq i \leq j \leq k \leq 4} r_{ijk} + \frac{Q}{D_2} \tag{7}$$

where r_i, r_{ij}, r_{ijk} denote the observed positive rates of single-channel,

pairwise-channel, and triple-channel combinations, respectively; D_2 represents the pairwise correction term; and Q denotes the higher-order correction term. Thus, P_{th} represents the theoretically expected positive rate for the decoded four-channel event. The full expanded form of the correction term is provided in the Supplementary Information. Based on P_{th}, the theoretical fluctuation scale δ_{th} was defined as:

$$\delta_{th} = -\frac{\sqrt{P_{th}}}{\ln(1-P_{th})\sqrt{N(1-P_{th})}} \tag{8}$$

where N denotes the total number of microchambers. The decoding confidence (CI) for the four-channel combination was then calculated as:

$$CI = \left| \frac{\ln\left(\frac{\ln(1-r_{1234})}{\ln(1-p_{th})}\right)}{\delta_{th}} \right| \tag{9}$$

where r_{1234} is the observed positive rate of the four-channel combination. A small CI value indicates better agreement between the observed decoding behavior and the theoretical expectation, whereas a larger value reflects greater deviation and therefore lower decoding consistency.

To complement this decoding-confidence assessment, the potential contribution of random co-partitioning was theoretically estimated from the positive-chamber fractions of the relevant lower-order encoding events. Assuming independent molecular partitioning, the expected co-positive rate arising solely from random co-partitioning between two events A and B can be expressed as P_random(A∩B) = P(A)×P(B).

For each decoded target, the absolute concentration was calculated using Poisson statistics based on the fraction of positive microchambers (Majumdar et al., 2017):

$$Concentration = -\frac{\ln\left(1-\frac{d_k}{n}\right)}{V_d} \tag{10}$$

where d_k is the number of positive microchambers assigned to target k, n is the total number of chambers, and V_d represents the effective volume of each microchamber. This formulation accounts for multiple molecules contributing to the same decoded target population, whereas potential composite codewords arising from co-partitioning were evaluated separately using the probabilistic analysis described above.

Notably, the proposed binary encoding framework changes the rule

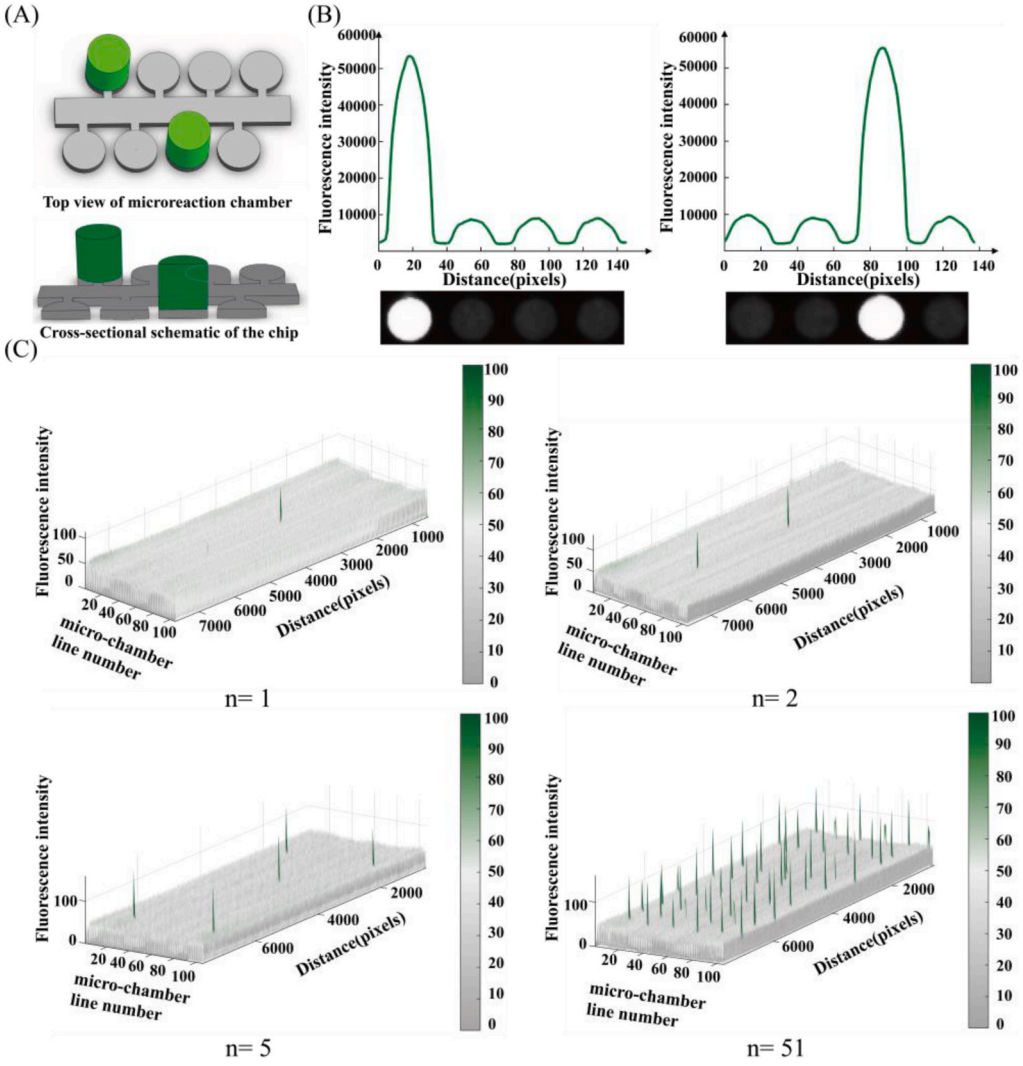

Fig. 2. Microchamber architecture as a fixed-partition structural model for deterministic spatial indexing. (A) Top-view and cross-sectional schematics of the validation chip containing predefined microchambers with different heights. (B) Representative fluorescence intensity profiles and corresponding local fluorescence images, showing spatially confined signal peaks with minimal inter-chamber spillover. (C) Three-dimensional fluorescence intensity maps for chamber architectures with increasing numbers of predefined fluorescence-signature chambers per repeating unit (n = 1, 2, 5, and 51), demonstrating preserved spatial periodicity and local peak localization across the array.

of target identification but does not alter the underlying Poisson-based quantification principle of digital PCR. In other words, multiplex expansion is achieved at the decoding level while the fundamental quantitative basis of dPCR is preserved. Quantitative experiments were performed in three independent technical replicates (n = 3). Each replicate used a separate quality-controlled, production-line-manufactured chip and involved independent sample loading, amplification, fluorescence imaging, and data analysis. Quantitative results are presented as mean ± SD unless otherwise specified.

3. Results and discussion

3.1. Microchamber architecture as a fixed-partition model for deterministic spatial indexing

To establish a controlled structural basis for validating partition identity consistency across fluorescence channels, we designed a set of cdPCR tool chips with predefined spatial organization and chamber occupancy patterns. As shown in Fig. 2A, the chip contained microchambers with two different heights. The gray chambers correspond to regular-height chambers (35 μm), whereas the green chambers represent chambers with a predefined height of 120 μm. By modulating chamber height in this manner, predefined high- and low-signal patterns could be introduced into the array, thereby generating spatially organized fluorescence signatures under imaging readout. These structures were not intended for routine detection assays, but rather served as controlled validation substrates for assessing whether chamber identity could be consistently preserved and recognized across fluorescence channels.

Representative fluorescence intensity profiles and corresponding local fluorescence images are shown in Fig. 2B. The high- and low-level chamber structures produced clearly distinguishable signal differences, thereby providing a visual representation of the preset chamber states in the fluorescence images. The resulting fluorescence peaks remained spatially confined with minimal spillover into adjacent chambers, indicating that the response of each individual chamber could be locally resolved with sufficient clarity. This feature is essential because reliable partition-resolved decoding requires not only channel-wise fluorescence readout, but also structurally separable signal localization at the level of individual partitions.

To further visualize the spatial organization of these validation chips, three-dimensional fluorescence intensity maps were generated for four representative chamber architectures containing predefined fluorescence signatures per repeating unit (n = 1, 2, 5, and 51; Fig. 2C). A comparison of the standard and engineered chip architectures and the corresponding fluorescence images are provided in Supplementary Fig. S2 and Supplementary Fig. S3, respectively. Across all tested structures, fluorescence peaks remained spatially ordered and clearly localized within the array. As the number of predefined positive chambers increased, the local signal distribution became denser, while the overall spatial periodicity and peak localization were preserved. These results indicate that the designed tool-chip architectures provide a stable and controllable fixed-partition model for subsequent validation of deterministic spatial indexing and cross-channel chamber identity consistency. More broadly, they define the structural basis by which fixed-partition dPCR systems can support partition-resolved binary

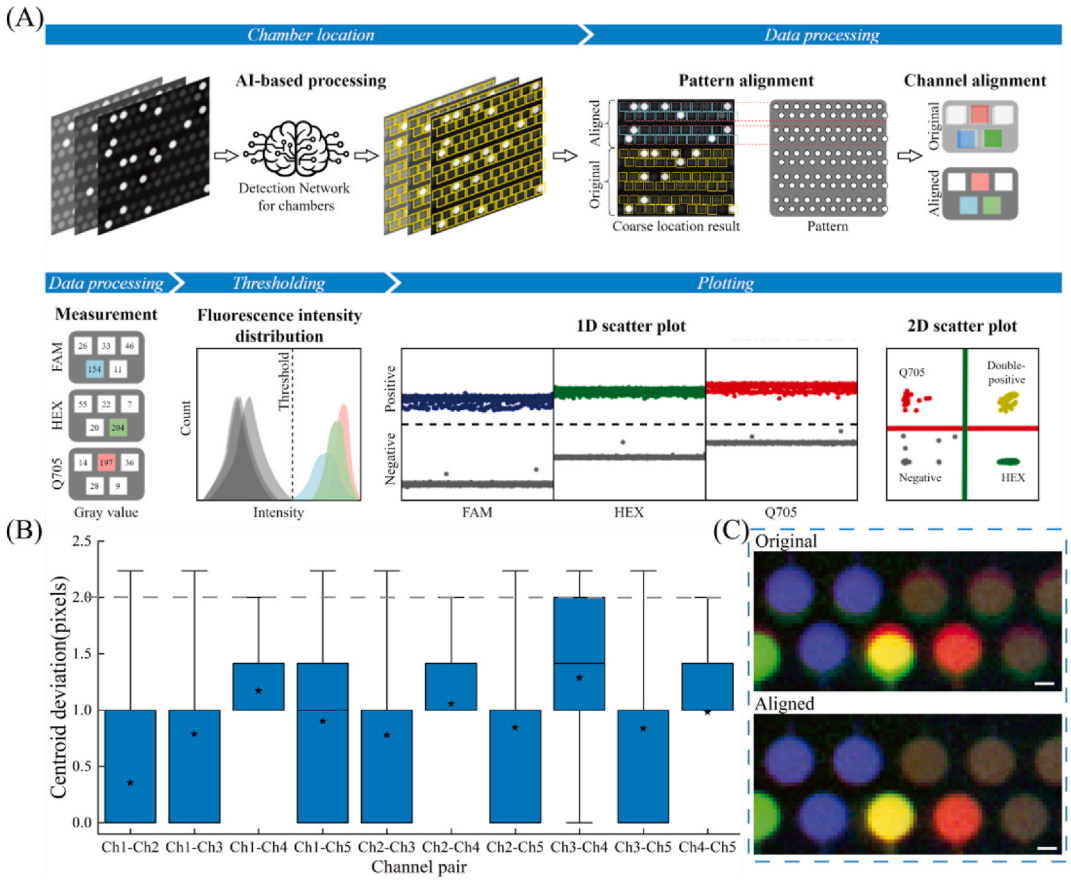

Fig. 3. Cross-channel chamber identity extraction and spatial consistency analysis for partition-resolved decoding. (A) Workflow for chamber localization and cross-channel alignment, including neural-network-based chamber detection, pattern registration, and spatial alignment to a unified coordinate system. (B) Distribution of centroid deviations between fluorescence channel pairs after alignment; the dashed line indicates the 2-pixel tolerance threshold. (C) Representative merged fluorescence images before and after spatial alignment, showing improved chamber correspondence after correction. Scale bar: 5 pixels.

encoding and decoding.

3.2. Cross-channel chamber identity consistency verification for partition-resolved decoding

Reliable partition-resolved binary decoding requires that the same physical partition be consistently recognized across different fluorescence channels. To establish such correspondence, we implemented a multi-step image processing workflow consisting of chamber localization, pattern registration, and cross-channel alignment, as illustrated in Fig. 3A. First, the spatial coordinates of individual chambers were identified using a neural-network-based chamber-detection method established in our previous work (Fan et al., 2025). The extracted chamber coordinates were then matched to a predefined chamber layout. Based on this spatial registration, fluorescence images acquired from different channels were further aligned to a unified coordinate system using a spatial alignment algorithm (details provided in Supplementary Section 3), thereby enabling direct chamber-to-chamber correspondence across spectral windows. Finally, an adaptive intensity threshold was determined per channel to classify each chamber as positive or negative, completing the partition-resolved binary decoding (details provided in Supplementary Section 4).

After chamber localization and alignment, cross-channel consistency was quantitatively evaluated by measuring centroid deviations between corresponding chambers. The distribution of centroid deviations for different channel pairs is summarized in Fig. 3B. Across all examined channel combinations, the median centroid deviation remained below 2 pixels, corresponding to less than 6.7% of the chamber diameter (~30 pixels). Because the residual registration error was far below the spatial scale of a single chamber, it was unlikely to cause chamber misassignment during channel-wise comparison.

Across 21,384 matched chambers, pairwise median, 95th-percentile, and 99th-percentile centroid deviations did not exceed 1.41, 2.24, and 3.16 pixels, respectively, and the maximum observed deviation was 5.10 pixels. The corresponding edge-field values were 1.41, 2.83, and 3.61 pixels, showing only a modest increase relative to the central field. No chamber reached the 16-pixel potential-misassignment boundary, giving a registration-failure rate of 0%. Detailed results are provided in Supplementary Fig. S5. Representative multi-channel fluorescence images before and after spatial alignment are shown in Fig. 3C. Before correction, subtle yet clearly discernible spatial shifts of 2–3 pixels were observed between corresponding chamber positions in different fluorescence channels. After alignment, the overlap between channels improved markedly, enabling more precise registration of individual chambers within the merged images. These observations confirm that the implemented localization and alignment strategy effectively reduced residual inter-channel offset and improved partition correspondence across the full field of view.

Taken together, these results demonstrate that the present cdPCR implementation can maintain cross-channel chamber identity with sufficient precision to support reliable partition-resolved binary decoding. More importantly, they define spatial consistency not merely as an imaging-quality metric, but as a core implementation requirement for any dPCR framework that seeks to combine spectral information with partition identity. In this sense, cross-channel geometric registration constitutes a methodological prerequisite for moving from analog fluorescence interpretation toward binary combinatorial decoding.

3.3. Binary spatial-spectral encoding and partition-resolved decoding in the cdPCR implementation

Having established that chamber identity could be preserved across fluorescence channels, we next demonstrated binary spatial-spectral decoding at the single-partition level within the cdPCR

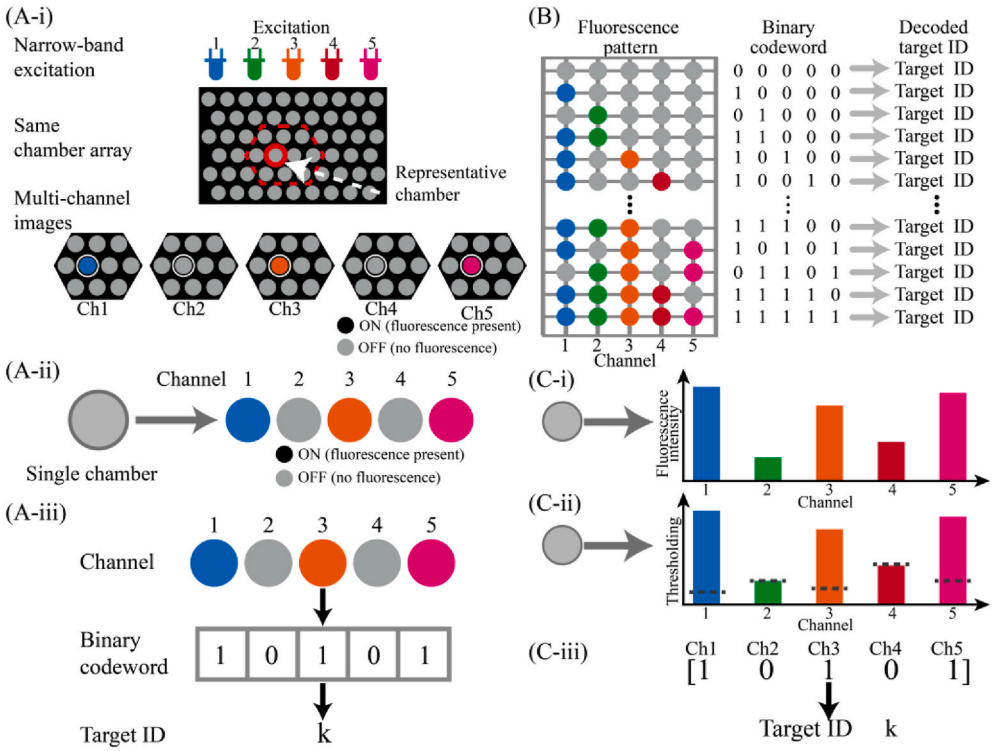

Fig. 4. Partition-resolved binary spatial-spectral encoding and chamber-level decoding strategy in the cdPCR implementation. (A) Sequential multi-channel excitation and fluorescence acquisition from the same microchamber array. (i) Multi-channel readout of identical spatially indexed chambers. (ii-iii) Conversion of channel-specific fluorescence states into chamber-level binary codewords. (B) Encoding matrix assigning unique binary codewords to predefined target identities. (C) Decoding workflow in which raw chamber fluorescence intensities (i) are thresholded (ii) and concatenated into binary activation patterns (iii) for target assignment. The five-channel schematic illustrates the generalized coding principle, whereas the application-level validation in this study used a four-channel implementation.

implementation. As shown in Fig. 4A–i, fluorescence images of the same microchamber array were sequentially acquired under narrow-band LED excitation at different wavelengths, thereby enabling direct cross-channel comparison of partitions sharing identical spatial indices. Under this framework, the fluorescence state of each chamber could be represented as a multi-channel activation pattern rather than an isolated single-channel intensity value.

For each chamber, channel-wise fluorescence signals were converted into binary ON/OFF assignments, as illustrated in Fig. 4A–ii and A-iii. Activated channels were assigned a value of "1," whereas non-activated channels were assigned "0," thereby generating a chamber-specific binary codeword. A predefined encoding matrix was then used to map these codewords to target identities (Fig. 4B). In this way, different targets were represented by distinct fluorescence activation patterns across channels, allowing multiple targets to be discriminated within the same partition array through codeword matching rather than through one-target-per-channel labeling alone.

The decoding workflow is shown in Fig. 4C. Raw chamber fluorescence intensities (Fig. 4C–i) were first measured across channels, then compared with channel-specific thresholds to generate binary activation states (Fig. 4C–ii), and finally concatenated into chamber-level codewords for target assignment (Fig. 4C–iii). Because decoding was performed on spatially indexed chambers, no spectral unmixing or pixel-wise classification was required. Instead, target identification was achieved by directly comparing the fluorescence state of the same physical partition across spectral windows.

These results demonstrate that fixed-position digital PCR can support binary spatial-spectral decoding through direct cross-channel comparison of the same physical partition. More broadly, they show that once partition identity is preserved, multiplex target assignment can be reformulated from a problem of analog intensity stratification into one of discrete combinatorial pattern recognition. This shift in decoding logic provides the conceptual basis for extending multiplex capacity beyond the conventional one-target-per-channel limit while reducing dependence on resolving multiple closely spaced fluorescence subclusters within a single channel.

3.4. *Application-level validation of binary spatial-spectral decoding by multiplex pathogen identification*

To evaluate the practical applicability of the proposed binary spatial-spectral encoding framework, we applied it to multiplex detection of respiratory pathogens using a four-channel cdPCR implementation. The assay targeted nine representative respiratory pathogens using pathogen-specific primer-probe sets (Supplementary Table S1). As summarized in Fig. 5A, each pathogen was assigned a predefined binary

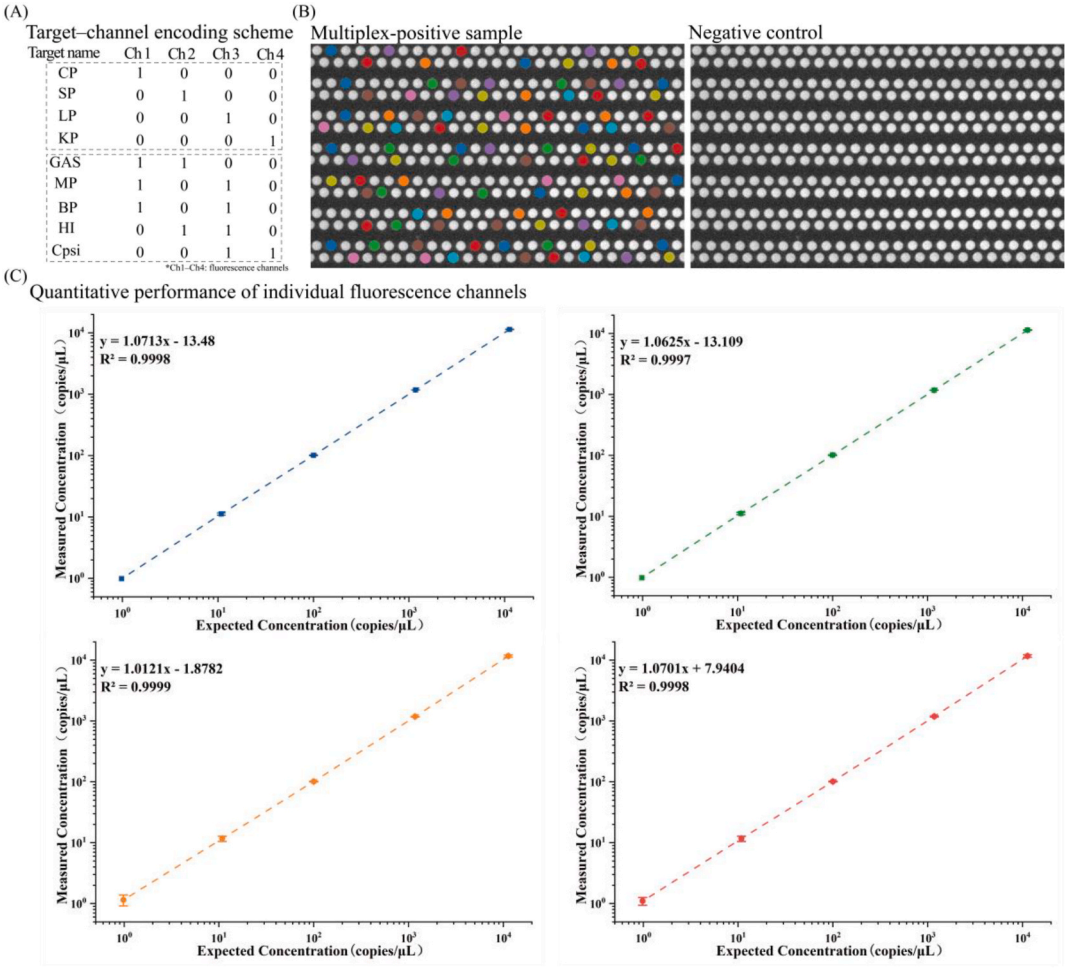

Fig. 5. Application-level validation of binary spatial-spectral decoding by multiplex respiratory pathogen detection. (A) Target-channel encoding matrix assigning unique binary codewords to nine respiratory pathogens in a four-channel implementation. (B) Representative decoded chamber maps for a multiplex-positive sample and a negative control. FColored chambers indicate successfully decoded target identities, whereas no decoded targets were observed in the negative control under the same decoding criteria. (C) Quantitative performance of individual fluorescence channels under multiplex assay conditions. Measured concentrations show strong linear correlations with expected input concentrations across four orders of magnitude, indicating preserved channel-level quantitative fidelity during combinatorial decoding. Pathogen abbreviations are defined in Methods Section 2.1, and the corresponding primer/probe sequences are provided in Supplementary Table S1.

codeword across four fluorescence channels. This design allowed the number of detectable targets to exceed the number of available spectral channels while preserving partition-level target identification.

Following digital PCR amplification and multi-channel imaging, decoding was performed at the microchamber level using the proposed strategy. Fig. 5B shows a representative decoded chamber map. In multiplex-positive samples, chambers assigned to different pathogen identities were successfully detected and displayed a spatially random distribution across the chip, indicating that distinct binary codewords could be resolved under the same amplification conditions. By contrast, no decoded target signals were observed in the negative control under the same decoding criteria, supporting the specificity of the encoding matrix and thresholding scheme and indicating the absence of obvious spurious combinatorial assignments in the present assay. The full-field no-template control and its channel-level fluorescence-amplitude distributions are provided in Supplementary Fig. S6.

To further assess whether combinatorial encoding altered channel-level quantitative behavior, regression analysis was performed independently for each fluorescence channel (Fig. 5C), with the corresponding positive chamber counts and calculated concentrations summarized in Supplementary Table S2. Across four orders of magnitude in input concentration, measured values showed strong linear correlations with expected concentrations, with slopes ranging from 1.01 to 1.07 and coefficients of determination between 0.9997 and 0.9999. These results indicate that the proposed framework supports multiplex pathogen identification without evident loss of channel-level quantitative fidelity.

Taken together, these data provide an application-level validation of the binary spatial-spectral decoding strategy under realistic multiplex assay conditions. The respiratory pathogen panel therefore serves not only as a use-case demonstration, but also as practical evidence that partition-resolved binary encoding can support reliable target discrimination under multiplex assay conditions while exceeding the conventional one-target-per-channel limit.

As an exploratory extension, a representative five-channel experiment further decoded 15 respiratory pathogen targets using five single-channel and ten dual-channel codewords, with the encoding matrix and target-level results provided in Supplementary Fig. S4 and Table S5.

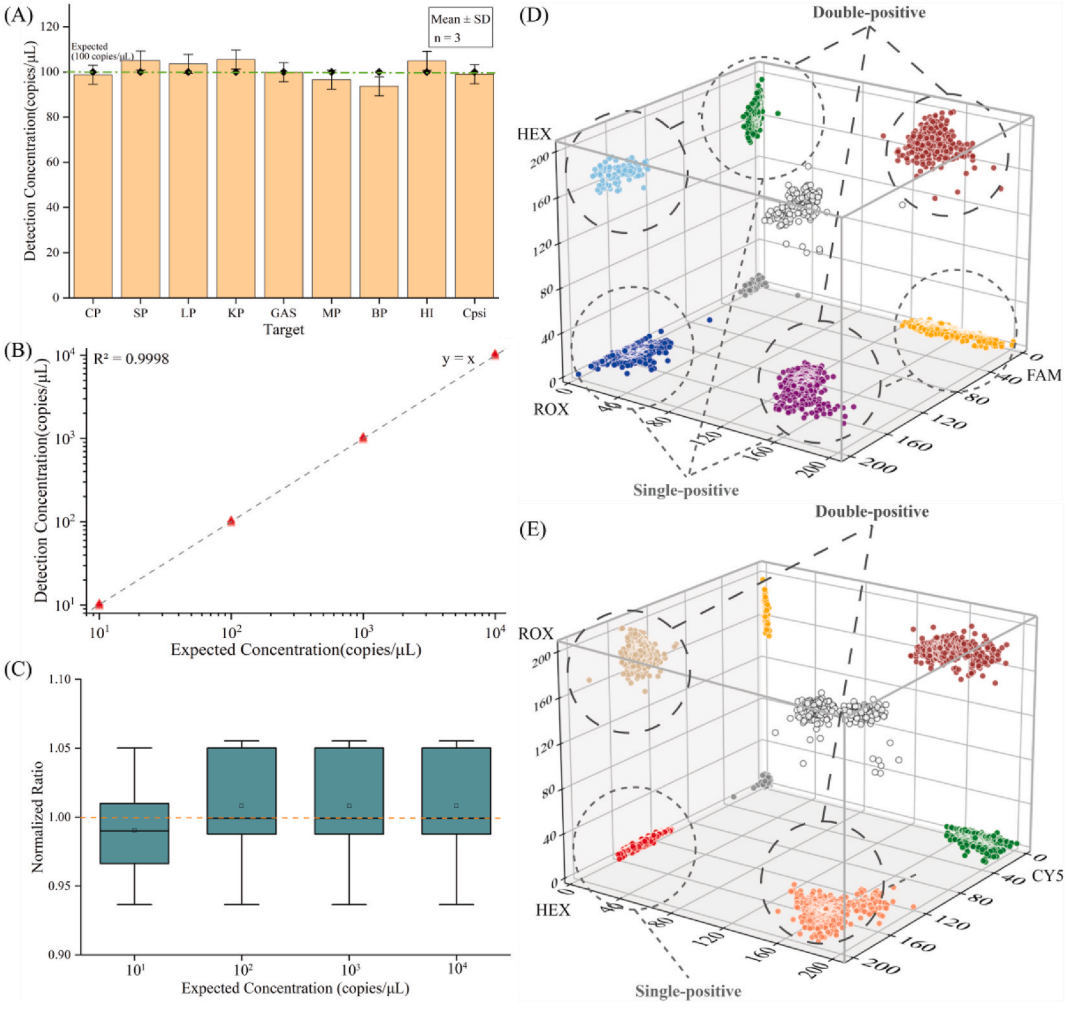

Fig. 6. Quantitative performance and fluorescence-pattern separability of the binary spatial-spectral decoding framework. (A) Measured concentrations of nine respiratory pathogen targets at an expected concentration of 100 copies/μL (mean ± SD, n = 3). (B) Linear regression analysis between expected and measured concentrations over four orders of magnitude (10^1-10^4 copies/μL). (C) Distribution of normalized concentration ratios (measured/expected) across different input concentrations. (D) Three-dimensional fluorescence intensity scatter plot showing clustering of fluorescence activation patterns across the FAM, HEX, and ROX channels. (E) Three-dimensional fluorescence intensity scatter plot showing clustering across the CY5, HEX, and ROX channels. These distributions are consistent with reliable binary decoding under the present experimental conditions. Colors correspond to decoded fluorescence activation patterns or target-associated codewords defined by the encoding matrix. (For interpretation of the references to color in this figure legend, the reader is referred to the Web version of this article.)

3.5. Quantitative performance of the binary spatial-spectral decoding framework

We next evaluated whether the proposed multiplexing strategy preserved the quantitative performance of digital PCR across different targets and input concentrations, as summarized in Fig. 6. At an expected concentration of 100 copies/μL, the measured concentrations of the nine respiratory pathogen targets remained close to the input values (Fig. 6A). The numbers of positive chambers and the corresponding concentrations calculated using Poisson statistics from three independent experiments are presented in Supplementary Table S3. The measured concentrations were centered near the expected value, with limited variation across replicates (n = 3), indicating good reproducibility and minimal target-dependent bias under multiplexed conditions.

The quantitative linearity of the system was further assessed over four orders of magnitude, ranging from 10^1 to 10^4 copies/μL (Fig. 6B). The measured concentrations obtained from repeated experiments are presented in Supplementary Table S4. Regression analysis revealed a strong linear relationship between expected and measured concentrations, with a coefficient of determination of $R^2 = 0.9998$. The close agreement with the ideal y = x relationship confirms that the proposed multiplexed cdPCR platform maintained accurate quantification across a broad dynamic range.

To further assess robustness across concentration levels, normalized concentration ratios (measured/expected) were summarized using box plots (Fig. 6C). Across all tested concentrations, the distributions remained centered near unity with limited spread, indicating minimal systematic deviation. In addition to target-level quantification, the separability of fluorescence signal combinations was evaluated using multi-dimensional fluorescence intensity analysis. Three-dimensional scatter plots constructed from fluorescence intensities across different channel combinations revealed visually distinct clusters corresponding to different fluorescence activation patterns, with limited apparent overlap (Fig. 6D and E). These distributions were consistent with reliable binary decoding under the present experimental conditions.

Taken together, these results show that binary spatial-spectral decoding expands multiplexing capacity while preserving the Poisson-based quantitative framework of dPCR. Compared with conventional PCR/qPCR, which remains advantageous for routine testing, the proposed cdPCR framework offers complementary benefits through partition-resolved multiplex identification and absolute quantification.

The present study represents a proof-of-concept implementation. Composite events matching assigned codewords may remain difficult to distinguish, particularly at high partition occupancy; concentrated samples should therefore be appropriately diluted. The corresponding low-abundance target-masking risk is analyzed in Supplementary Fig. S8. The simulated throat-swab matrix and extracted nucleic acid results support applicability to complex sample workflows (Supplementary Fig. S7), although broader clinical validation remains necessary. Finally, while 2^N-1 defines the theoretical codeword capacity, practical performance depends on codeword selection and assay compatibility. The systematically evaluated four-channel nine-target assay and exploratory five-channel 15-target experiment demonstrate the current performance and scalability of the framework, respectively (Supplementary Fig. S4 and Table S5).

4. Conclusions

In this work, we developed a binary spatial-spectral encoding and decoding strategy for ultra-multiplexed digital PCR. Unlike conventional multiplexing approaches that mainly rely on analog fluorescence stratification, the proposed framework assigns target identities through partition-resolved binary ON/OFF codewords derived from the same spatially indexed partition across channels. Rather than encoding targets solely through predefined color combinations, this strategy converts multi-channel fluorescence readout into an identity-preserving combinatorial decoding problem, thereby providing a scalable route for multiplex detection beyond the number of available fluorescence channels.

Using fixed-position cdPCR as the first implementation platform, we demonstrated that stable chamber identity could be maintained across fluorescence channels, enabling reliable chamber-resolved decoding over the full field of view. With only four fluorescence channels, the system achieved simultaneous detection of nine respiratory pathogens and maintained accurate quantification over four orders of magnitude, with an R^2 value of 0.9998. These results validate the feasibility of binary spatial-spectral decoding for expanding the multiplexing capacity of digital PCR while preserving its Poisson-based quantitative foundation. The consumable cost of the proposed cdPCR platform is approximately $4 per chip. Moreover, multiplex detection on a single chip avoids the use of separate chips for individual targets, thereby reducing the overall consumable cost.

Importantly, the proposed strategy is not intrinsically restricted to cdPCR. Its broader applicability depends on whether partition identity can be preserved, recovered, or tracked during multi-channel readout. Although validated here using fixed-position cdPCR, the framework may therefore be extended to other digital PCR platforms, including microwell-based systems and ddPCR, through reliable cross-channel partition tracking or re-identification. Future work will focus on developing these capabilities, together with error-tolerant codebooks, threshold standardization, and improved assay compatibility.

CRediT authorship contribution statement

Jinrong Shen: Formal analysis, Software, Validation, Writing – original draft, Writing – review & editing. **Jingxing Fan:** Data curation, Software, Writing – review & editing. **Gangwei Xu:** Data curation, Methodology. **Zhehao Zhao:** Conceptualization, Resources. **Haofeng Li:** Investigation, Validation. **Dongping Wu:** Funding acquisition, Methodology, Project administration.

Declaration of competing interest

The authors declare that they have no known competing financial interests or personal relationships that could have appeared to influence the work reported in this paper.

Acknowledgments

This work was supported by Prevention and Control of Emerging and Major Infectious Diseases-National Science and Technology Major Project: 2026ZD01912700, the National Natural Science Foundation of China: 62374044.

Appendix A. Supplementary data

Supplementary data to this article can be found online at https://doi.org/10.1016/j.bios.2026.118952.

Data availability

Data will be made available on request.

References

Baker, M., 2012. Digital PCR hits its stride. Nat. Methods 9 (6), 541–544.
Basu, A.S., 2017. Digital assays part I: partitioning statistics and digital PCR. SLAS TECHNOLOGY: Translating Life Sciences Innovation 22 (4), 369–386.
Busato, F., Ursuegui, S., Deleuze, J.-F., Tost, J., 2025. Multiplex digital PCR for the simultaneous quantification of a miRNA panel. Anal. Chim. Acta 1335, 343440.
Cao, Y., Wang, J., Jiang, Y., Xu, L., Tian, Y., Fan, Z., Pan, Z., Mo, Y., Zhu, X., Zhang, X., 2025. Multiplex droplet digital PCR for the detection and quantitation of Streptococcus pneumoniae, Mycoplasma pneumoniae, and Haemophilus influenzae. Front. Cell. Infect. Microbiol. 15, 1548492.

de Korne-Elenbaas, J., Caduff, L., Lison, A., McLeod, R., Pitton, M., Gan, C., Julian, T.R., 2025. Design, validation, and implementation of multiplex digital PCR assays for simultaneous quantification of multiple targets. Lett. Appl. Microbiol. 78 (1) ovae137.

Denis, J.A., Patroni, A., Guillerm, E., Pepin, D., Benali-Furet, N., Wechsler, J., Manceau, G., Bernard, M., Coulet, F., Larsen, A.K., Karoui, M., Lacorte, J.M., 2016. Droplet digital PCR of circulating tumor cells from colorectal cancer patients can predict KRAS mutations before surgery. Mol. Oncol. 10 (8), 1221–1231.

Fan, J., Shen, J., Zhao, Z., Xu, G., Wu, D., 2025. R3Net: a three-phase neural network for noise elimination and accurate quantification in chip-based digital PCR. Sensor. Actuator. B Chem. 442, 138123.

Gaňová, M., Zhang, H., Zhu, H., Korabečná, M., Neužil, P., 2021. Multiplexed digital polymerase chain reaction as a powerful diagnostic tool. Biosens. Bioelectron. 181, 113155.

Heyries, K.A., Tropini, C., VanInsberghe, M., Doolin, C., Petriv, O.I., Singhal, A., Leung, K., Hughesman, C.B., Hansen, C.L., 2011. Megapixel digital PCR. Nat. Methods 8 (8), 649–651.

Huang, Y., Gao, Z., Ma, C., Sun, Y., Huang, Y., Jia, C., Zhao, J., Feng, S., 2023. An integrated microfluidic chip for nucleic acid extraction and continued cdPCR detection of pathogens. Analyst 148 (12), 2758–2766.

Huggett, J.F., Cowen, S., Foy, C.A., 2015. Considerations for digital PCR as an accurate molecular diagnostic tool. Clin. Chem. 61 (1), 79–88.

Kokkoris, V., Vukicevich, E., Richards, A., Thomsen, C., Hart, M.M., 2021. Challenges using droplet digital PCR for environmental samples. Appl. Microbiol. 1 (1), 74–88.

Lau, B.T., Wood-Bouwens, C., Ji, H.P., 2017. Robust multiplexed clustering and denoising of digital PCR assays by data gridding. Anal. Chem. 89 (22), 11913–11917.

Li, C., Kang, N., Ye, S., Huang, W., Wang, X., Wang, C., Li, Y., Liu, Y.F., Lan, Y., Ma, L., 2024. All-in-one OsciDrop digital PCR system for automated and highly multiplexed molecular diagnostics. Adv. Sci. 11 (21), 2309557.

Li, H., Bai, R., Zhao, Z., Tao, L., Ma, M., Ji, Z., Jian, M., Ding, Z., Dai, X., Bao, F., 2018. Application of droplet digital PCR to detect the pathogens of infectious diseases. Biosci. Rep. 38 (6). BSR20181170.

Majumdar, N., Banerjee, S., Pallas, M., Wessel, T., Hegerich, P., 2017. Poisson plus quantification for digital PCR systems. Sci. Rep. 7 (1), 9617.

McDermott, G.P., Do, D., Litterst, C.M., Maar, D., Hindson, C.M., Steenblock, E.R., Legler, T.C., Jouvenot, Y., Marrs, S.H., Bemis, A., 2013. Multiplexed target detection using DNA-Binding dye chemistry in droplet digital PCR. Anal. Chem. 85 (23), 11619–11627.

Miotke, L., Lau, B.T., Rumma, R.T., Ji, H.P., 2014. High sensitivity detection and quantitation of DNA copy number and single nucleotide variants with single color droplet digital PCR. Anal. Chem. 86 (5), 2618–2624.

Mirabile, A., Sangiorgio, G., Bonacci, P.G., Bivona, D., Nicitra, E., Bonomo, C., Bongiorno, D., Stefani, S., Musso, N., 2024. Advancing pathogen identification: the role of digital PCR in enhancing diagnostic power in different settings. Diagnostics 14 (15), 1598.

Morcia, C., Carrara, I., Ghizzoni, R., Terzi, V., Bolli, G., Chiusa, G., 2024. Chip digital PCR (cdPCR) to identify and quantify botrytis cinerea infection in tomatoes. Horticulturae 10 (1), 91.

Olmedillas-López, S., Olivera-Salazar, R., García-Arranz, M., García-Olmo, D., 2022. Current and emerging applications of droplet digital PCR in oncology: an updated review. Mol. Diagn. Ther. 26 (1), 61–87.

Sanders, R., Huggett, J.F., Bushell, C.A., Cowen, S., Scott, D.J., Foy, C.A., 2011. Evaluation of digital PCR for absolute DNA quantification. Anal. Chem. 83 (17), 6474–6484.

Santos-Barriopedro, I., Ursuegui, S., Fradet, E., Dangla, R., 2023. Robust higher-order multiplexing in digital PCR by color-combination. bioRxiv, 2023.2005.2010.540190.

Schlenker, F., Kipf, E., Borst, N., Hutzenlaub, T., Zengerle, R., von Stetten, F., Juelg, P., 2021. Virtual fluorescence color channels by selective photobleaching in digital PCR applied to the quantification of KRAS point mutations. Anal. Chem. 93 (30), 10538–10545.

Shen, J., Fan, J., Zhao, Z., Hou, Z., Xu, G., Wu, D., 2025. Chip-based digital PCR with large-field one-shot imaging for high-sensitivity nucleic acid quantification. Biosens. Bioelectron. 279, 117381.

Shen, J., Zheng, J., Li, Z., Liu, Y., Jing, F., Wan, X., Yamaguchi, Y., Zhuang, S., 2021. A rapid nucleic acid concentration measurement system with large field of view for a droplet digital PCR microfluidic chip. Lab Chip 21 (19), 3742–3747.

Si, H., Xu, G., Jing, F., Sun, P., Zhao, D., Wu, D., 2020. A multi-volume microfluidic device with no reagent loss for low-cost digital PCR application. Sensor. Actuator. B Chem. 318, 128197.

Suo, T., Liu, X., Feng, J., Guo, M., Hu, W., Guo, D., Ullah, H., Yang, Y., Zhang, Q., Wang, X., 2020. ddPCR: a more accurate tool for SARS-CoV-2 detection in low viral load specimens. Emerg. Microb. Infect. 9 (1), 1259–1268.

Tan, L.L., Loganathan, N., Agarwalla, S., Yang, C., Yuan, W., Zeng, J., Wu, R., Wang, W., Duraiswamy, S., 2023. Current commercial dPCR platforms: technology and market review. Crit. Rev. Biotechnol. 43 (3), 433–464.

Trypsteen, W., Vynck, M., De Neve, J., Bonczkowski, P., Kiselinova, M., Malatinkova, E., Vervisch, K., Thas, O., Vandekerckhove, L., De Spiegelaere, W., 2015. ddpcRquant: threshold determination for single channel droplet digital PCR experiments. Anal. Bioanal. Chem. 407 (19), 5827–5834.

Velez, D.O., Mack, H., Jupe, J., Hawker, S., Kulkarni, N., Hedayatnia, B., Zhang, Y., Lawrence, S., Fraley, S.I., 2017. Massively parallel digital high resolution melt for rapid and absolutely quantitative sequence profiling. Sci. Rep. 7 (1), 42326.

Vogelstein, B., Kinzler, K.W., 1999. Digital pcr. Proc. Natl. Acad. Sci. 96 (16), 9236–9241.

Vynck, M., Chen, Y., Gleerup, D., Vandesompele, J., Trypsteen, W., Lievens, A., Thas, O., De Spiegelaere, W., 2023. Digital PCR partition classification. Clin. Chem. 69 (9), 976–990.

Whale, A.S., Huggett, J.F., Cowen, S., Speirs, V., Shaw, J., Ellison, S., Foy, C.A., Scott, D. J., 2012. Comparison of microfluidic digital PCR and conventional quantitative PCR for measuring copy number variation. Nucleic Acids Res. 40 (11) e82-e82.

Wu, J., Tang, B., Qiu, Y., Tan, R., Liu, J., Xia, J., Zhang, J., Huang, J., Qu, J., Sun, J., 2022. Clinical validation of a multiplex droplet digital PCR for diagnosing suspected bloodstream infections in ICU practice: a promising diagnostic tool. Crit. Care 26 (1), 243.

Xu, G., Si, H., Jing, F., Sun, P., Zhao, D., Wu, D., 2020. A double-deck self-digitization microfluidic chip for digital PCR. Micromachines 11 (12), 1025.

Xu, G., Yang, H., Qiu, J., Reboud, J., Zhen, L., Ren, W., Xu, H., Cooper, J.M., Gu, H., 2023. Sequence terminus dependent PCR for site-specific mutation and modification detection. Nat. Commun. 14 (1), 1169.

Yin, J., Xia, L., Zou, Z., Zhuang, J., Mu, Y., 2022. A direct and multiplex digital PCR chip for EGFR mutation. Talanta 250, 123725.

Zhong, Q., Bhattacharya, S., Kotsopoulos, S., Olson, J., Taly, V., Griffiths, A.D., Link, D. R., Larson, J.W., 2011. Multiplex digital PCR: breaking the one target per color barrier of quantitative PCR. Lab Chip 11 (13), 2167–2174.

Zhou, H., Liu, D., Ma, L., Ma, T., Xu, T., Ren, L., Li, L., Xu, S., 2020. A SARS-CoV-2 reference standard quantified by multiple digital PCR platforms for quality assessment of molecular tests. Anal. Chem. 93 (2), 715–721.

Zhu, Q., Xu, Y., Qiu, L., Ma, C., Yu, B., Song, Q., Jin, W., Jin, Q., Liu, J., Mu, Y., 2017. A scalable self-priming fractal branching microchannel net chip for digital PCR. Lab Chip 17 (9), 1655–1665.

Zonta, E., Garlan, F., Pecuchet, N., Perez-Toralla, K., Caen, O., Milbury, C., Didelot, A., Fabre, E., Blons, H., Laurent-Puig, P., 2016. Multiplex detection of rare mutations by picoliter droplet based digital PCR: sensitivity and specificity considerations. PLoS One 11 (7), e0159094.